INT. J. NUM. METH. HEAT FLUID FLOW, VOL. 3, 233–244 (1993)

ON THE ENTHALPY METHOD

C. R. SWAMINATHAN* AND V. R. VOLLER†

Departments of Mechanical Engineering and Civil & Mineral Engineering†, University of Minnesota, Minneapolis, MN 55455, USA*

ABSTRACT

Two common fixed grid enthalpy methods used in the numerical modelling of phase change problems are the apparent heat capacity and the source based methods. In this paper, a general enthalpy method that includes as subsets both apparent heat capacity and source based methods, is derived. Following this, an optimal enthalpy scheme is identified. The superiority of the optimal scheme over the apparent heat capacity and the source based schemes is illustrated by solving sample phase change problems.

KEY WORDS Enthalpy method Phase change problems

INTRODUCTION

The key feature in a phase change problem is the presence of a moving boundary (or region) on which heat and mass balance conditions have to be met. A popular approach in the numerical modelling of such problems is the so-called 'enthalpy' method. The major advantage of this method is that despite the presence of moving boundaries, the problem is cast in a conservative form that allows for the solution to be obtained on a fixed space grid. There are a variety of ways in which the enthalpy method can be implemented[1]. Two common variations are: (1) the apparent heat capacity methods[2–4], in which the non-linearity associated with the evolution of latent heat is accounted for using a modified heat capacity term, and (2) the source based methods[5–8], in which the latent heat evolution is represented by a suitable source term.

The objective of this paper is to present a general enthalpy method that will encompass a wide range of the alternative methods previously presented in the literature. Particular attention will be directed at apparent heat capacity and source based methods. The focus in this paper will be on the essential mechanics of the phase change algorithm. Consequently a major portion of the paper will be devoted to the numerical treatment of the energy equation, in particular the handling of the latent heat evolution associated with the phase change. In the first instance, a conduction driven phase change problem will be considered. Later, applications to problems that involve fluid flow and mushy phase change regions will also be demonstrated. Before the general approach is proposed, the appropriate governing equations and a brief outline of apparent heat capacity and source based methods will be provided.

GOVERNING EQUATIONS

In a fluid undergoing a liquid to solid phase transformation (i.e., solidification), the conservation of energy can be written down in terms of the mixture enthalpy H as:

$$\frac{\partial(\rho H)}{\partial t} + \nabla\cdot(\rho \mathbf{u} H) = \nabla\cdot(k\nabla T) \tag{1}$$

0961–5539/93/030233–12$2.00

Received August 1992
Revised December 1992

where ρ is the density, $\mathbf{u}$ is the velocity, T is temperature, and k is the conductivity. A reasonably general definition for the mixture enthalpy is[1]:

$$H = (1-g)\int_{T_{ref}}^{T} c_s \, d\alpha + g\int_{T_{ref}}^{T} c_l \, d\alpha + gL \tag{2}$$

where the subscripts $[\ ]_s$ and $[\ ]_l$ refer to solid and liquid respectively, T_{ref} is a reference temperature, c is the specific heat, g is the volume fraction of liquid and L is the latent heat associated with the phase change. A representative enthalpy–temperature (H–T) curve is shown in *Figure 1*. Note that this representative enthalpy–temperature relationship allows for both an isothermal phase change (depicted as a discontinuity in the H–T curve) as well as a mushy (solid/liquid) phase change that occurs over a temperature range.

In problems involving convection effects, in addition to the energy equation, one has to consider the equations for mass conservation, viz.:

$$\frac{\partial \rho}{\partial t} + \nabla\cdot(\rho \mathbf{u}) = 0 \tag{3}$$

and momentum conservation, viz.:

$$\frac{\partial(\rho \mathbf{u})}{\partial t} + \nabla\cdot(\rho \mathbf{u}\mathbf{u} - \mu\nabla\mathbf{u}) + \nabla p - \mathbf{S} = 0 \tag{4}$$

where μ is the viscosity, p is the pressure and $\mathbf{S}$ is a source term.

For clarity in presentation of the various enthalpy schemes, we shall restrict initial discussions to problems with constant thermophysical properties driven by conduction alone. This simplification will in no way limit the application of the enthalpy schemes discussed. Under these assumptions the governing equation (1) reduces to:

$$\rho\frac{\partial H}{\partial t} = \nabla\cdot(k\nabla T) \tag{5}$$

with the enthalpy H defined as:

$$H = cT + gL \tag{6}$$

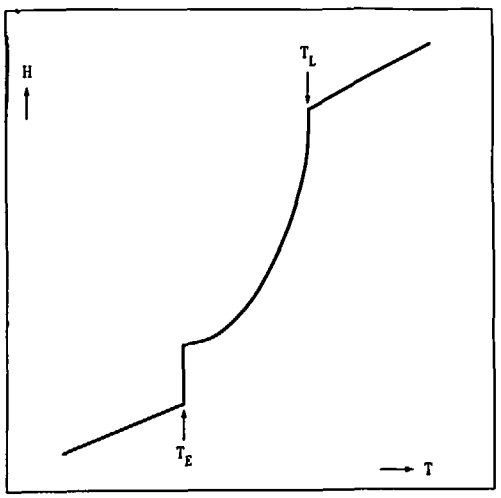

Figure 1 A representative enthalpy–temperature relationship

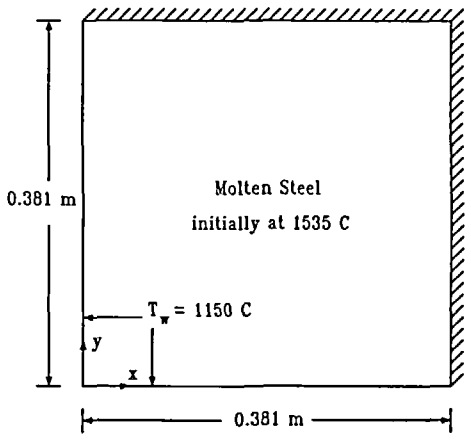

Figure 2 Solidification of a steel ingot: problem specification

TWO COMMON ENTHALPY METHODS

In order to fully illustrate the generalized enthalpy scheme, we shall first discuss the numerical mechanics of two existing classes of enthalpy methods. Although we recognize that this is a familiar territory for a number of readers, we have included it here for the sake of completeness.

Apparent heat capacity methods

In apparent heat capacity methods, (5) is rewritten as[2]:

$$\rho C^{\text{app}} \frac{\partial T}{\partial t} = \nabla \cdot (k \nabla T) \tag{7}$$

where $C^{\text{app}} = \mathrm{d}H/\mathrm{d}T$ is called the apparent heat capacity. The major advantage of (7) is that it is similar in form to the standard heat conduction equation. On using a fully implicit time integration scheme, the control volume[9] or finite element[10] discrete analog of (7) can be written as:

$$[a_p + (\rho C^{\text{app}} V)_p] T_p^{m+1} = (\rho C^{\text{app}} V)_p T_p^{\text{old}} + \sum_{nb} a_{nb} T_{nb}^{m+1} \tag{8}$$

where the a's represent the coefficients of the discretization equation. The subscripts $[\ ]_p$ and $[\ ]_{nb}$ represent the node point p and the neighbour nodes respectively, while the superscripts $[\ ]^{m+1}$ and $[\ ]^{\text{old}}$ represent the iteration level and the old time value respectively. The term V is used to represent the spacial volume associated with a node. Note that (8) assumes a lumped capacitance formulation[10] for the finite element scheme. In evaluating the coefficients in (8), the apparent heat capacity C^{app} can be obtained using one of many approximations, examples include:

(1) those based on space averaging, e.g., the method proposed by Lemmon[3],

$$C^{\text{app}} = \left[\frac{\nabla H \cdot \nabla H}{\nabla T \cdot \nabla T} \right]^{1/2} \tag{9}$$

(2) those based on temporal averaging, e.g., the method proposed by Morgan *et al.*[4],

$$C^{\text{app}} = \left[\frac{H^m - H^{\text{old}}}{T^m - T^{\text{old}}} \right] \tag{10}$$

If the H–T relation involves a step discontinuity, application of the apparent heat capacity method will require a finite phase change temperature interval. In a basic implementation, if this interval is chosen too small, unless sufficient care is taken in the choice of the time step, it is possible to miss out some of the latent heat effects[11]. This problem can be avoided and the performance of the apparent heat capacity method greatly enhanced by using a post-iterative correction scheme[11]. In this procedure, after the calculation of the $(m + 1)$th temperature solution, the current enthalpy values are obtained from:

$$H^{m+1} = H^{\text{old}} + C^{\text{app}} [T^{m+1} - T^{\text{old}}] \tag{11}$$

This step allows for the ready identification of node points that are changing phase. Before the next iteration, the temperature at these nodes is adjusted to be consistent with the calculated enthalpy values using the given H–T curve. The post-iterative correction step ensures a heat balance over the time interval and avoids any latent heat from being missed out. On convergence, the post iterative correction procedure will arrive at discrete temperature and enthalpy fields that will satisfy the appropriate discrete form of the enthalpy equation (5).

Source based methods

In source based methods, a direct substitution of (6) into (5) is made so that:

$$\rho c \frac{\partial T}{\partial t} = \nabla \cdot (k \nabla T) - \rho L \frac{\partial g}{\partial t} \tag{12}$$

The discrete analog of (12) can be written as:

$$[a_p + (\rho cV)_p] T_p^{m+1} = (\rho cV)_p T_p^{\text{old}} + \sum_{nb} a_{nb} T_{nb}^{m+1} + (\rho LV)_p [g_p^{\text{old}} - g_p^m] \tag{13}$$

After each iterative calculation of the temperature field, the liquid fraction is updated via:

$$g_p^{m+1} = g_p^m + \lambda \, \text{corr} \tag{14}$$

where λ is a relaxation factor. In practice, this update is followed by an undershoot/overshoot correction[7] so as to ensure that the liquid fraction is within the bounds of 0 and 1. The application of (14) is similar to the post-iterative correction used in the apparent heat capacity methods and on convergence ensures a full heat balance over the time interval. A number of possible relations for 'corr' in (14) have been proposed in the literature[5–8]; examples include, but are not limited to:

(1) the fictitious heat source method[5],

$$\text{corr} = \frac{c}{L} [T_p^{m+1} - T_p^m] \tag{15}$$

(2) the Brent *et al.* method[7],

$$\text{corr} = \frac{a_p + (\rho cV)_p}{(\rho LV)_p} [T_p^{m+1} - T_p^m] \tag{16}$$

Note that in using either of these corrections, if the phase change is occurring at node p, i.e., $0 < g_p^m < 1$, the value of T_p^{m+1} is forced to be consistent with the appropriate phase change value on the H–T curve before the next iteration is commenced.

A GENERAL METHOD

The starting point in the derivation of the general method is the direct discrete analog of (5), i.e.,

$$a_p T_p^{m+1} = \sum_{nb} a_{nb} T_{nb}^{m+1} + (\rho V)_p [H_p^{\text{old}} - H_p^{m+1}] \tag{17}$$

Equation (17) is solved using the following predictor–corrector procedure at each iteration step.

Predictor step

On expanding the enthalpy as:

$$H_p^{m+1} = H_p^* + \left. \frac{\mathrm{d}H}{\mathrm{d}T} \right|_{H_p} [T_p^{m+1} - T_p^*] \tag{18}$$

(17) can be written in the linear form:

$$(a_p - S_p) T_p^{m+1} = \sum_{nb} a_{nb} T_p^{m+1} + S_c \tag{19}$$

where

$$S_p = -(\rho V)_p \left.\frac{dH}{dT}\right|_{H_p}$$
$$S_c = (\rho V)_p \left[H_p^{old} - H_p^* + \left.\frac{dH}{dT}\right|_{H_p} T_p^* \right] \tag{20}$$

Equation (19) is solved for the current temperature field, T_p^{m+1}.

Corrector step

The enthalpy is updated from the current temperature field via

$$H_p^{m+1} = H_p^* + \left.\frac{dH}{dT}\right|_{H_p} [T_p^{m+1} - T_p^*] \tag{21}$$

Following this the temperature at node points that are changing phase is corrected to be consistent with H_p^{m+1} on the appropriate H–T curve.

The proposed general enthalpy method is ideally designed for problems in which there is a unique enthalpy–temperature relationship. Such a condition covers a very wide class of phase change problems[12]. Further it is assumed that at any point in the phase change range (specified by the enthalpy–temperature pair H^* and T^*), the derivative dH/dT is well defined.

On choosing different approximations for the dH/dT term and appropriate setting of H_p^* and T_p^*, the proposed general approach can be used to represent both apparent heat capacity and source based methods. For example, the substitutions:

$$H_p^* = H_p^{old}$$
$$T_p^* = T_p^{old} \tag{22}$$
$$\left.\frac{dH}{dT}\right|_{H_p} = \frac{H_p^m - H_p^{old}}{T_p^m - T_p^{old}} = C^{app}$$

in the two step general scheme will lead immediately to the Morgan apparent heat capacity scheme with a post-iterative correction ((8) and (11) above). Alternatively the substitutions:

$$H_p^* = H_p^m$$
$$T_p^* = T_p^m \tag{23}$$
$$\left.\frac{dH}{dT}\right|_{H_p} = c$$

along with the use of (6) will lead to the fictitious heat source method* ((13)–(15) above).

AN OPTIMUM APPROACH

The above examples clearly illustrate how the proposed scheme can readily be used to represent a number of apparent heat capacity or source based methods. The examples also illustrate the commonality between apparent heat capacity and source based schemes. Having devised a general scheme, the key question to ask is whether there is an optimal approach? In other words, can we arrive at a particular choice for H_p^*, T_p^* and dH/dT that would ensure optimal convergence

* Note that in this derivation, the relationship $H_p^{m+1} = cT_p^m + g_p^{m+1}L$ has been assumed in the enthalpy update

on all phase change systems alike? In deriving the apparent heat capacity and source based method from the general scheme, an approximation was employed for the slope of the H–T curve (i.e., for dH/dT). In many phase change systems the form of the H–T curve is known and the exact slope at a given point can be calculated. Recently, the authors[12] have proposed that the optimum version of the general scheme will be the one that uses the exact replacement for dH/dT, i.e., the substitutions:

$$\begin{aligned} H_p^* &= H_p^m \\ T_p^* &= T_p^m \\ \left.\frac{dH}{dT}\right|_{H_p} &= \text{slope of the } H\text{–}T \text{ curve at } H_p^m \end{aligned} \tag{24}$$

will ensure optimal convergence. Note that at discontinuities in the H–T curve the slope dH/dT can be accurately approximated using an arbitrarily large value (e.g., 10^8). The performance of the optimal enthalpy scheme on a range of phase change problems will be demonstrated below.

A PERFORMANCE COMPARISON

In the first instance, the solidification of steel in a mould will be taken as a test problem. Molten steel is held in a long, square (0.762 m × 0.762 m) mould at a temperature $T_i = 1535°C$, which is above the liquidus temperature of $T_L = 1502.5°C$. At time zero, the mould walls are held at the temperature $T_M = 1150°C$, which is below the solidus temperature of $T_S = 1497.5°C$. As time progresses, a solid shell and a solid/liquid mushy region ('sandwiched' between the T_L and T_S isotherms) move inward from the mould walls. The evolution of latent heat in the mushy region is assumed to be linear (i.e., the slope of the H–T curve is a constant in the phase change interval). If fluid flow and end effects are neglected and symmetry is applied, the problem is governed by (5) applied to the two-dimensional quarter mould cross-section. The model problem with the thermophysical properties is summarized in *Figure 2* and *Table 1* respectively.

In essence, this test problem is a variation of the well known freezing in a corner problem[13] and the accuracy of the enthalpy formulation on this problem is well documented. In the current case, the objective is to use this test problem to compare the performance of the variations of the proposed general scheme. In this performance testing, a finite difference approximation on a uniform 41 × 41 space grid and a time step of 261.29 sec (corresponding to a discrete Fourier number of 16) will be used. The performance of three schemes is investigated: (1) the Morgan scheme (22), (2) the fictitious heat source scheme (23), and (3) the optimal scheme (24). *Table 2* summarizes the total number of iterations and CPU time on an IBM PC for 20 time steps of simulation for the three schemes. *Figure 3* shows the convergence pattern in terms of the normalized L_2 norm of the residual of the discrete energy equation for the three schemes. This numerical experiment clearly shows the performance advantage of the optimal enthalpy scheme.

Further insight into the mechanisms and performance of the various schemes can be obtained on considering the iterative relationships between the temperature and enthalpy. *Figure 4* schematically illustrates the iterative progress of temperature and enthalpy at a particular node during a given time step. In this example, at the start of the time step, the consistent value of the enthalpy–temperature pair (H_p^{old}, T_p^{old}) are assumed to be outside of the phase change interval (point 'a'). The initial iterative predictor–corrector steps are identical for all the three schemes. In effect, the iterative value of the temperature obtained from the predictor step will be located on the extension of the liquid H–T slope (slope PQ). This is depicted by point 'b' in the Figure. Before the next iteration, the enthalpy is updated and the temperature is made consistent with the H–T curve. The corrected value of temperature is denoted by point 'c'. It is from this point

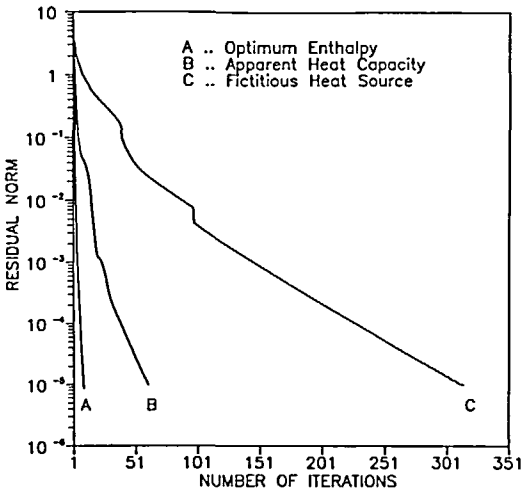

Figure 3 Solidification of a steel ingot: convergence characteristics of the three enthalpy schemes at a representative time step

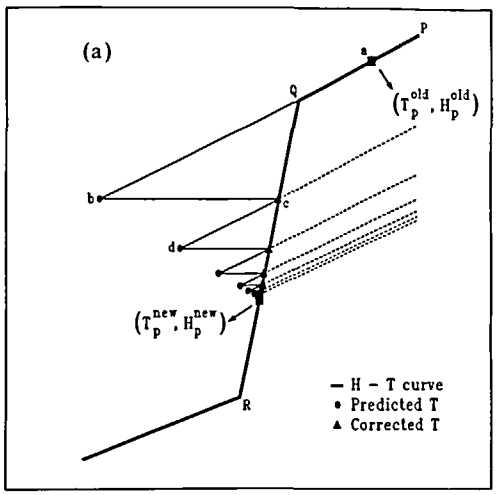

Figure 4 A schematic illustration of the iterative progress of temperature and enthalpy at a particular node during a given time step: (a) the fictitious heat source method

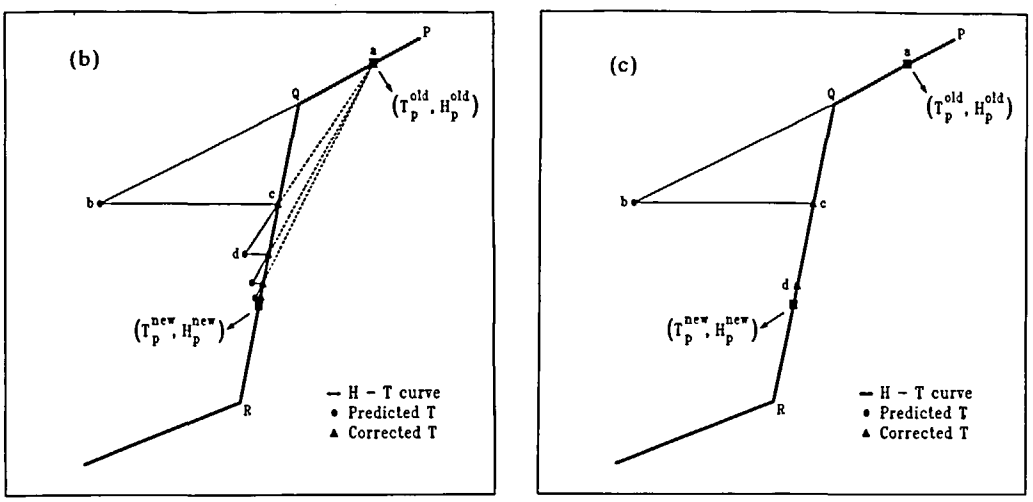

Figure 4 A schematic illustration of the iterative progress of temperature and enthalpy at a particular node during a given time step: (b) the apparent heat capacity method, and (c) the optimal enthalpy method

onwards that the three methods begin to differ. We shall consider each of the three methods in turn:

1. Fictitious heat source method (*Figure 4a*): In the fictitious heat source method, during the next iteration, the predicted temperature value will lie on a line passing through the point 'c' with a slope equal to the slope of the liquid H–T curve (i.e., slope PQ). Next, the enthalpy is updated and the temperature is made consistent with the H–T curve. This procedure continues until convergence. Clearly the speed of convergence is controlled by the difference in the slopes of line PQ and QR. When over-relaxation is used in the fictitious heat source method, the chosen slope will in effect be steeper and convergence should improve.

Table 1 Solidification of a steel ingot: thermophysical properties and boundary and initial conditions

Conductivity, k	30.0 W/m °C
Specific heat, c	750 J/kg °C
Density, ρ	7200.0 kg/m^3
Latent heat, L	262.5 kJ/kg
Solidus temperature, T_S	1497.5°C
Liquidus temperature, T_L	1502.5°C
Initial temperature, T_i	1535.0°C
Mould wall temperature, T_w	1150.0°C

Table 2 Performance of enthalpy schemes in terms of the number of iterations and CPU requirement for 20 time steps of simulation on an IBM 386 25 MHz machine

Method	No. of iterations*	CPU (sec)
Apparent heat capacity	1267	2387.97
Fictitious heat source	6519	12708.39
Optical enthalpy	182	361.30

*The convergence criteria is a normalized residual tolerance of 10^{-5}

2. Apparent heat capacity method (*Figure 4b*): In the apparent heat capacity method, during the next iteration, the predicted temperature value will lie on a line passing through the point 'c' with a slope equal to the slope of line ac (i.e., $(H_p^m - H_p^{\text{old}})/(T_p^m - T_p^{\text{old}})$). Clearly the slope becomes progressively steeper and one would expect the convergence to be faster than the fictitious heat source method. In essence, the method can be viewed as a fictitious heat source method with adaptive over-relaxation.

3. Optimal enthalpy method (*Figure 4c*): In the optimal method, however, since the exact slope (i.e. slope QR) is picked, the iteration path will be confined to the H–T curve and convergence will be very rapid.

Before leaving this test problem it is important to note that for a given convergence tolerance, the results from each of the three schemes were close to identical. Also on the scale of the problem, the chosen freezing range of 5°C can be considered to be very small and the problem is close to an isothermal problem. It is stressed, however, that in using the optimal scheme this range could have been made arbitrarily small (e.g., 10^{-8}). Such a choice, however, made very little difference to the results.

A PROBLEM WITH FLUID FLOW

Next we consider the solidification of an aluminium alloy in the presence of natural convection in the melt. Three different latent heat evolution mechanisms are investigated as shown in *Figure 5*. Curve A corresponds to an isothermal solidification (e.g., an alloy of eutectic composition). Curves B and C correspond to a mushy region solidification. In curve B, the latent heat is assumed to evolve linearly. Usmani *et al.*[14] have solved this problem using an unequal order finite element method. In curve C, the latent heat is assumed to evolve in a non-linear fashion (e.g., the Scheil equation[15]). Curve C corresponds to an Al–4.5% Cu alloy and all thermophysical properties for the problem are consistent with this alloy. A columnar dendritic solidification morphology is assumed such that the solid velocity in the mushy region is zero. Under this assumption, the governing enthalpy equation reduces to:

$$\frac{\partial(\rho H)}{\partial t} + \nabla\cdot(\rho \mathbf{u} T) = \nabla\cdot(k\nabla T) \tag{25}$$

The model problem with all the thermophysical properties and enthalpy–temperature relationship is summarized in *Figure 6* and *Tables 3* and *4*.

In the first instance, a control volume finite difference discretization with a staggered grid arrangement[9] is used. The SIMPLER algorithm[9] is used to solve the discrete momentum and

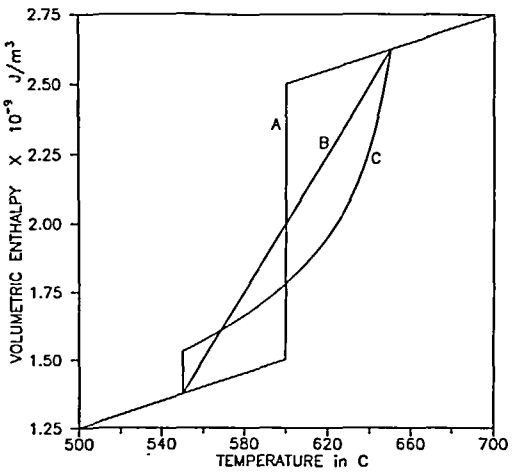

Figure 5 Three different latent heat evolution mechanisms for aluminium alloys

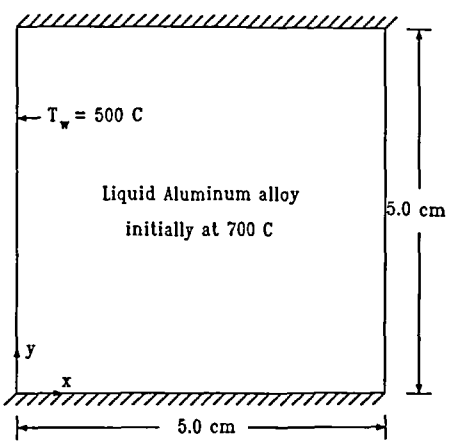

Figure 6 Solidification of an aluminium alloy in the presence of natural convection: problem specification

Table 3 Solidification of an aluminium alloy in the presence of natural convection: thermophysical properties and boundary and initial conditions

Conductivity, k	100.0 W/m °C
Specific heat, c	1000.0 J/kg °C
Density, ρ	2500.0 kg/m^3
Latent heat, L	400.0 kJ/kg
Viscosity, μ	0.0025 kg/m s
Coefficient of thermal expansion, β	4.0×10^{-5}
Initial temperature, T_i	700.0°C
Wall temperature, T_w	500.0°C
Eutectic temperature, T_E (curve A)	600.0°C
Solidus temperature, T_S (curve B)	550.0°C
Eutectic temperature, T_E (curve C)	550.0°C
Liquidus temperature, T_L (curve B, C)	650.0°C
Melting point of aluminium, T_{Al}	675.0°C
Partition coefficient, κ	0.14

Table 4 Solidification of an aluminium alloy in the presence of natural convection: enthalpy–temperature relation in the phase change region for the three curves A, B and C

Curve	Enthalpy–temperature relationship	
A	$cT_E \leqslant H \leqslant cT_E + L$	if $T = T_E$
B	$H = cT + \left[\dfrac{T - T_S}{T_L - T_S}\right]L$	if $T_S \leqslant T \leqslant T_L$
C	$cT_E \leqslant H \leqslant cT_E + g_E L$	if $T = T_E$; $g_E = 0.1539$
	$H = cT + gL$	if $T_E < T \leqslant T_L$; $g = \left[\dfrac{T_{Al} - T}{T_{Al} - T_L}\right]^{-1/(1-\kappa)}$

continuity equations. The enthalpy–porosity technique of Brent *et al.*[7] is used to model the flow in the mushy region. In this model, the source term S in the momentum equations takes the form[7]:

$$\mathbf{S} = -\frac{C(1-g)^2}{g^3}\mathbf{u} + \rho\,\mathbf{grav}\,\beta[T - T_{\text{ref}}] \tag{26}$$

where C is the morphological constant, β is the coefficient of thermal expansion, and **grav** is the acceleration due to gravity. In essence the flow in the mushy region is made to mimic flow in a porous media and the velocities in the system approach zero as the full solid region is reached. The second term on the right hand side of (26) is a result of the Boussinesq approximation. The enthalpy–porosity technique of modelling flow in the mushy region has been experimentally validated in the case of melting of a block of gallium[7].

In the computational runs a 30×30 grid of uniform control volumes is used. The under-relaxation factor in the momentum equations is set to 0.8. The time step size is varied from 0.04 to 1.96 sec in a linear manner. In addition, when using the apparent heat capacity approach, a phase change temperature interval of 1°C was used at discontinuities in the enthalpy–temperature curve. Further details on the implementation of the enthalpy methods can be found in References 7 and 12.

Table 5 summarizes the performance results of the computation in terms of the number of iterations and CPU time on the CRAY-YMP for 25 time steps of simulation. Two different convergence criteria were used: a maximum mass imbalance of 10^{-4} for the momentum equations and a maximum absolute difference in the sum of the liquid fraction field of 10^{-4} for the energy equation. The results indicate that:

1. the optimal enthalpy approach outperforms the apparent heat capacity and the fictitious heat source method for all choices of latent heat evolution mechanisms;
2. on the isothermal test problem, the fictitious heat source method is relatively slower compared to the other two methods because the approximation for the slope is a severe under-estimation of the actual slope in the phase change range. The convergence can be significantly improved if the enthalpy update (21) is over-relaxed, e.g. with a value of $\lambda = 5$, the number of iterations were reduced from 2362 to 665;
3. on the linear test problem, the performance of all the schemes are almost identical since the slopes outside and inside of the phase change region are relatively close in value, i.e., 1000 as against 5000.

The enthalpy porosity model has also been implemented in the unequal order control volume finite element scheme of Ramadhyani[16]. This technique uses special exponential shape functions[17] for the velocity and the temperature variable and the standard bilinear shape function for the pressure variable. The resulting discrete equations are solved using the SIMPLER algorithm[9]. Full details on this finite element scheme can be found in Ramadhyani[16]. The performance

Table 5 Performance comparison of enthalpy schemes implemented in a control volume finite difference discretization in terms of the number of iterations and CPU requirement for 25 time steps of simulation on the CRAY-YMP supercomputer

	Apparent heat capacity		Fictitious heat source		Optimal enthalpy	
Problem	No. of iterations	CPU (sec)	No. of iterations	CPU (sec)	No. of iterations	CPU (sec)
A. Isothermal	897	66.758	2362	172.396	432	33.069
B. Linear	367	28.698	448	34.781	326	25.904
C. Scheil	571	52.369	1264	97.212	326	27.057

Table 6 Performance comparison of enthalpy schemes implemented in a control volume finite element discretization in terms of the number of iterations and CPU requirement for 25 time steps of simulation on the CRAY-YMP supercomputer

	Apparent heat capacity		Fictitious heat source		Optimal enthalpy	
Problem	No. of iterations	CPU (sec)	No. of iterations	CPU (sec)	No. of iterations	CPU (sec)
A. Isothermal	976	834.032	3131	2527.611	555	474.250
B. Linear	358	304.732	441	371.817	326	278.572
C. Scheil	485	417.946	1400	1130.504	345	294.090

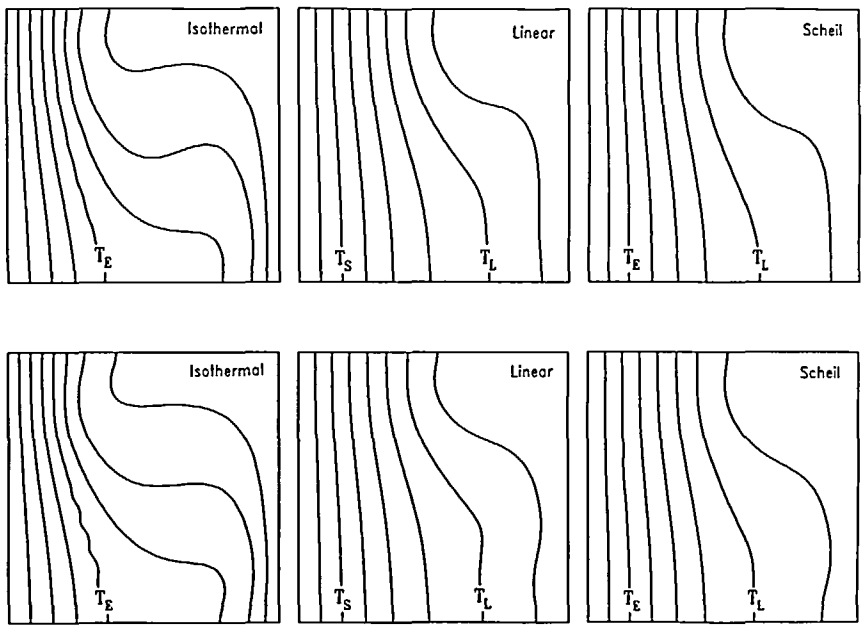

Figure 7 Solidification of an aluminium alloy in the presence of natural convection: isotherm plots for curves A, B and C using control volume finite difference (top panel) and control volume finite element (bottom panel) formulations. The isotherms are 25°C apart

results, based on a uniform 30 × 30 grid (corresponding to 961 velocity nodes and 256 pressure nodes) are shown in *Table 6*. The under-relaxation factors, the time step and the convergence criteria are the same as that used in the finite difference implementation. A key feature in these results as compared to the finite difference results is an order of magnitude increase in the CPU requirements. This is due in part to the current overhead required to solve the finite element equations. Once again as clearly shown in *Table 6*, the optimal enthalpy method outperforms the apparent heat capacity and the fictitious heat source method.

Figure 7 compares the isotherms obtained using the finite difference and finite element schemes for each of the chosen H–T curves. The comparison can be considered to be reasonable.

CONCLUSIONS

The objective of this paper has been to provide a comprehensive and unifying treatment of enthalpy methods for phase change problems. The major contributions have been: (1) the introduction of a generalized predictor–corrector scheme that encompasses many existing schemes, (2) the identification of an optimal scheme, and (3) a graphical demonstration of the iteration paths of various enthalpy schemes.

The optimal enthalpy scheme is compared to the apparent heat capacity scheme and the fictitious heat source scheme on a pure conduction driven problem as well as on problems involving natural convection. Both isothermal and mushy phase change problems have been considered. The comparison indicates the superiority of the optimal scheme. Although the test problems considered are relatively simple, the enthalpy methods covered by the umbrella of the proposed general scheme are readily applicable to more complex and practical phase change problems.

ACKNOWLEDGEMENTS

This work was supported by the National Center for Excellence in Metalworking Technology, operated by Concurrent Technologies Corporation (formerly Metalworking Technology, Inc.), Johnstown (Pennsylvania, USA) under contract to the US Navy as part of the US Navy Manufacturing Technology Program. Computational time on the CRAY-YMP was provided by the Minnesota Supercomputer Institute (MSI), Minneapolis.

REFERENCES

1 Voller, V. R., Swaminathan, C. R. and Thomas, B. G. Fixed grid technique for phase change problems: a review, *Int. J. Num. Meth. Eng.*, **30**, 875–898 (1990)
2 Comini, G., Del Giudice, S., Lewis, R. W. and Zienkiewicz, O. C. Finite element solution of nonlinear heat conduction problems with special reference to phase change, *Int. J. Num. Meth. Eng.*, **8**, 613–624 (1974)
3 Lemmon, E. C. Phase change techniques for finite element codes, in *Proc. Conf. on Numerical Methods in Thermal Problems* (Eds R. W. Lewis and K. Morgan), Pineridge Press, Swansea, pp. 149–158 (1979)
4 Morgan, K., Lewis, R. W. and Zienkiewicz, O. C. An improved algorithm for heat conduction problems with phase change, *Int. J. Num. Meth. Eng.*, **12**, 1191–1195 (1978)
5 Rolph, W. D. III and Bathe, K. J. An efficient algorithm for analysis of nonlinear heat transfer with phase change, *Int. J. Num. Meth. Eng.*, **18**, 119–134 (1982)
6 Roose, J. and Storrer, O. Modelization of phase changes by fictitious heat flow, *Int. J. Num. Meth. Eng.*, **20**, 217–225 (1984)
7 Brent, A. D., Voller, V. R. and Reid, K. J. Enthalpy porosity technique for modelling convection–diffusion phase change: application to the melting of a pure metal, *Num. Heat Transfer*, **13B**, 297–318 (1988)
8 Voller, V. R. and Swaminathan, C. R. General source-based method for solidification phase change, *Num. Heat Transfer*, **19B**, 175–190 (1991)
9 Patankar, S. V. *Numerical Heat Transfer and Fluid Flow*, Hemisphere, Washington DC (1980)
10 Zienkiewicz, O. C. and Taylor, R. L. *The Finite Element Method*, 4th Edn, Vol. 1, McGraw-Hill, New York (1989)
11 Comini, G., Del Giudice, S. and Saro, O. A conservative algorithm for multidimensional conduction phase change, *Int. J. Num. Meth. Eng.*, **30**, 697–709 (1990)
12 Swaminathan, C. R. and Voller, V. R. A general enthalpy method for modeling solidification processes, *Metall. Trans.*, **23B**, 651–664 (1992)
13 Thomas, B. G., Samarasekara, I. V. and Brimacombe, J. K. Comparison of numerical modeling techniques for complex two-dimensional, transient heat conduction problems, *Metall. Trans.*, **15B**, 307–318 (1984)
14 Usmani, A. S., Lewis, R. W. and Seetharamu, K. N. Natural convection controlled change of phase, *Int. J. Num. Meth. Fluids*, **15**, 1023–1035 (1991)
15 Flemings, M. C. *Solidification Processing*, McGraw-Hill, New York, pp. 160–163 (1974)
16 Ramadhyani, S. Solution of the equations of convective heat, mass and momentum transfer by the finite-element method using quadrilateral elements, *PhD Thesis*, University of Minnesota, Minneapolis (1979)
17 Ramadhyani, S. and Patankar, S. V. Solution of the convection–diffusion equation by a finite-element method using quadrilateral elements, *Num. Heat Transfer*, **8**, 595–612 (1985)